

Trade Science Inc.

# Nano Science and Nano Technology

*An Indian Journal*

**Full Paper**

NSNTAIJ, 2(1), 2008 [30-36]

## Copper-oxide nano-particles dopings for promoted micro-structural and transport properties of $Pb_{1-x}Cu_xZrO_3$ regime

Morsy M.A.Sekkina, Khaled M.Elsabawy\*, Marwa M.Bediwy  
Chemistry Department, Faculty of Science, Tanta University, Tanta-31527, (EGYPT)

E-mail: ksabawy@yahoo.com, ksabawy@hotmail.com

Received: 3<sup>rd</sup> March, 2008 ; Accepted: 8<sup>th</sup> March, 2008

### ABSTRACT

The samples having the general formula  $Pb_{1-x}Cu_xZrO_3$  perovskite regime were synthesized carefully via solid state reaction rout (where  $x = 0.0, 0.05, 0.1, 0.2, 0.25, 0.4, 0.5, 0.6$  and 1mole). Many investigations were performed including structural, micro structural (SEM) and thermal analysis (TGA& DTA) which carried out on green mixture. The prepared samples were found to have semiconducting feature with minimum activation energy  $1.98 \times 10^{-4}$  eV. The estimated grain size were found to be in between 80 and 150 nm. Furthermore, Infrared- absorption spectra recorded show broad-to medium peaks lies at I( $400-600\text{cm}^{-1}$ ), II( $250-400\text{cm}^{-1}$ ) and III( $150-250\text{ cm}^{-1}$ ). Finally, EPR spectra were recorded for pure- and variant Cu-doped perovskite giving broad signal which is good indication to  $\text{Cu}^{+2}$ -ion existence.

© 2008 Trade Science Inc. - INDIA

### KEYWORDS

Nano-dopings;  
Perovskite  $PbZrO_3$ ;  
X-ray diffraction;  
SE-microscopy;  
Thermal analyses;  
DC-electrical conductivity;  
ESR-spectra.

### INTRODUCTION

Most of the compounds with the general formula  $ABO_3$  have the perovskite structure<sup>[1]</sup> in which "A" may be a mono-, di-, or tri-valent cation and "B" may be a penta-, tetra-, or tri-valent cation<sup>[2]</sup>.

Solid solutions of lead zirconate-titanate ( $PbZrO_3$ - $PbTiO_3$  system) attract the attention of researchers and developers in various fields of science and technology because of their potential applications in memories, microwave tunable capacitors, microelectromechanical systems (MEMS), pyroelectric sensors and electro-optical switches<sup>[3-12]</sup>. It was reported that the antiferroelectric (AFE) to ferroelectric transition leads to significant energy storage for a dc field. This feature of  $PbZrO_3$  makes it a candidate material for energy

storage applications<sup>[13]</sup>.

Preparation of lead zirconate or (PZ) by conventional processes requires the use of high temperatures at which  $\text{PbO}$  volatility becomes significant. It was reported that the full development of pure  $PbZrO_3$  phase occurs after sintering at temperatures above  $1200^\circ\text{C}$  for at least 2h in controlled  $\text{PbO}$  atmospheres<sup>[14-17]</sup>.

PZ powders can also be prepared by wet-chemistry based process routs, which include chemical coprecipitation<sup>[18,19]</sup>, microemulsion<sup>[20]</sup> and Sol-gel technique<sup>[17]</sup>.

Bernd et al.<sup>[21]</sup> prepared PZT thin films by the deposition sol slurry, this method consists of a PZT-sol on acetic acid basis and PZT powder. Furthermore, Kong et al.<sup>[22]</sup> prepared PZ by a high-energy ball milling process using oxides as starting materials.

Bharadwaja et al.<sup>[23]</sup> studied the X-ray diffraction (XRD) for lead zirconate and La-doped lead zirconate thin films and reported that pure lead zirconate thin films showed a pseudo-cubic (110) orientation, whereas all the La-modified films showed a pseudo-cubic (111) orientation. The XRD analysis for lead lanthanum zirconate titanate (PLZT) thin films has been studied<sup>[24]</sup> and showed that the PLZT thin films are polycrystalline and the lattice parameter a decrease slightly with increasing La concentrations.

Boutarfaia<sup>[25]</sup> studied XRD, differential thermal analysis (DTA) and thermal gravimetric analysis (TGA) for  $x\text{PbZrO}_3-(0.95-x)\text{PbTiO}_3-0.05\text{Pb}(\text{Fe}_{1/5},\text{Ni}_{1/5},\text{Sb}_{3/5})\text{O}_3$ , it was reported that, the endothermic peak observed at about 240°C is due to  $\text{Pb}_3\text{O}_4$  decomposition and a appreciable weight loss of 2.5% is found with TGA, and another endothermic signal at 560°C which is related to  $\text{Pb}_3\text{O}_4$  final decomposition.

The scanning electron microscope (SEM) has been studied<sup>[19]</sup> for  $\text{PbZrO}_3$  and showed the submicrometer and spherical nature of the  $\text{PbZrO}_3$  powder.

Akimov<sup>[26]</sup> studied the IR spectra of lead zirconate-titanate with a rhombohedral and a tetragonal strucrures and it has been established that with increase in the content of lead titanate in solid solutions of lead zirconate-titanate with a tetragonal structure, the frequency of the ferroelectric- active mode shifts toward higher frequencies.

The essential goal of present article is studying the effect of copper dopings or/ substitution on the A-site of perovskite on:

- (a) Structural and microstructural properties of lead zirconate ( $\text{PbZrO}_3$ ) regime.
- (b) Transport properties, Magnetic order and spectral properties.

## **EXPERIMENTAL**

### **Samples perparation**

The pure lead zirconate ( $\text{PbZrO}_3$ ) and doped samples with general formula ( $\text{Pb}_{1-x}\text{Cu}_x\text{ZrO}_3$ ) where ( $x=0.05, 0.1, 0.2, 0.25, 0.4, 0.5, 0.6$  and 1 mole) were prepared by the conventional solid state reaction route and sintering procedure using appropiate amounts of  $\text{Pb}_3\text{O}_4$ ,  $\text{ZrO}_2$  and  $\text{CuCO}_3$  each of purity >99%. The

mixture was grinding in an agate mortar for 1h. Then the finely ground powder were subject to firing at 800°C for 20 hrs and reground and finally pressed into pellets with (thickness 0.2cm and diameter 1.2cm).

Sintering process was carried out at 850°C for 48 hrs. Then the furance is cooled slowly down to room temperature. 10% more off-stoichiometric  $\text{Pb}_3\text{O}_4$  were used in order to compensate lead deficient which is due to its sublimation during sintering process.

It is well known that, the particles size of  $\text{CuO}$  and  $\text{ZrO}_2$  resulted from thermal or/hydrothermal sintering process will be in the range of 10-50 nm specially after mechanical milling as mentioned in many previously reported articles like<sup>[27]</sup>. So the dopings will be in the range of nano-dopings powders.

### **Structural measurements**

The X-ray diffraction measurements (XRD) were carried out at room temperature on the fine ground samples on the range ( $2\theta=15-75^\circ$ ) using Cu-K $\alpha$  radiation source and a computerized [Shimadzu (Japan)] X-ray diffractometer with two theta scan technique.

Scanning electron microscope (SEM) measurements were carried out using small pieces of the prepared samples on different sectors to be accurate to the actual molar ratios by using “JXA-840A, JEOL-Japan”.

### **DC-electrical conductivity measurements**

The DC-electrical conductivity were measured as a function of absolute temperature using the two-probe technique. Measurements were carried out from room to elevated temperatures up to 500°C.

### **Thermal analyses measurements**

The thermogravimetric analysis (TGA) and the differential thermal analysis (DTA) measurements were carried out on the green mixtures of the prepared samples using a computerized Shimadzu (Japan) TGA/ DTA analyzer and  $\text{Al}_2\text{O}_3$  as reference for DTA measurements.

### **Solid infrared absorption spectra measurements**

The IR absorption spectra of the samples were recorded using “Perkin Elmer” Infrared Spectrophotometer Germany in the range 200-1500  $\text{cm}^{-1}$  using spec. Pure KBr matrix.

# Full Paper

## Magnetic measurements

The electron spin resonance spectra (ESR) were recorded at x-band frequencies on a "Bruker-Germany" ESR Spectrometer at room temperature at the National Research Center, Egypt. The magnetic field was swept from 0 to over 8 KG and the calibrated energy was 1 KG with a digital gaussmeter. Several selected samples were investigated.

## RESULTS AND DISCUSSION

Figure (1<sub>a-k</sub>) displays the X-ray diffraction patterns of pure lead zirconate ( $PbZrO_3$ ) and Cu-doped PZ regime having general formula ( $Pb_{1-x}Cu_xZrO_3$ ) where ( $x=0.05, 0.1, 0.2, 0.25, 0.4, 0.5, 0.6$  and 1 mole).

Analysis of the corresponding  $2\theta$  values and the interplanar spacings  $d$  ( $\text{\AA}$ ) by using computerized programme proved that, the compound is mainly belongs to orthorhombic crystal structure, that expressed by assigned peaks.

The unit cell dimensions were calculated using the parameters of the most intense X-ray reflection peaks and found to be  $a = 7.7042\text{\AA}$ ,  $b = 12.09\text{\AA}$  and  $c = 6.6345\text{\AA}$  for the pure  $PbZrO_3$ . Even though PZ was first reported to be tetragonal<sup>[28]</sup> at room temperature, single-crystal studies revealed the structure to be orthorhombic<sup>[29]</sup>.

The present XRD Patterns of PZ are in full agreement with results reported by Fang et al.<sup>[30]</sup> and Kong et al.<sup>[22]</sup>. They reported and confirmed that the lead zirconate regime crystallize to yield an orthorhombic crystal form regardless the type of processing or techniques of preparation. Only the % gradient of phase formed might changed according to the type of preparation techniques applied (solid state- solution route or emulsion, etc).

It was observed that  $c$ -axis exhibits slight length compression by increasing Cu-content on the basis of ionic size radius as shown in figure (2), the ionic radius of Cu-ion smaller than that of Pb-ion such that,  $Cu^{2+} = 57\text{pm}$  while  $Pb^{2+} = 78\text{pm}$ .

From figure (1<sub>a-k</sub>) One can notifies that orthorhombic phase kept as it is without change from  $x = 0.0$  till  $x = 0.25$  mole while the most intense reflection peaks in the range of doping ratio  $0.25 \leq x < 1$  represent orthor-

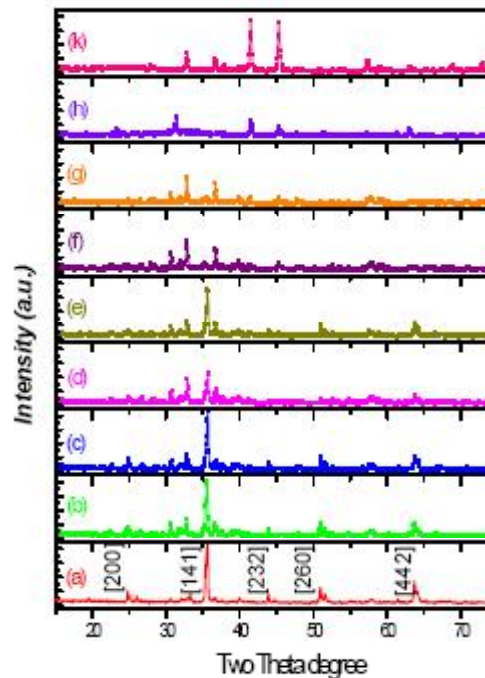


**Figure 1(a-k):** The obtained room temperature XRD patterns for the prepared (a)  $PbZrO_3$ , (b)  $Pb_{0.95}Cu_{0.05}ZrO_3$ , (c)  $Pb_{0.9}Cu_{0.1}ZrO_3$ , (d)  $Pb_{0.8}Cu_{0.2}ZrO_3$ , (e)  $Pb_{0.75}Cu_{0.25}ZrO_3$ , (f)  $Pb_{0.6}Cu_{0.4}ZrO_3$ , (g)  $Pb_{0.5}Cu_{0.5}ZrO_3$ , (h)  $Pb_{0.4}Cu_{0.6}ZrO_3$  and (k)  $CuZrO_3$

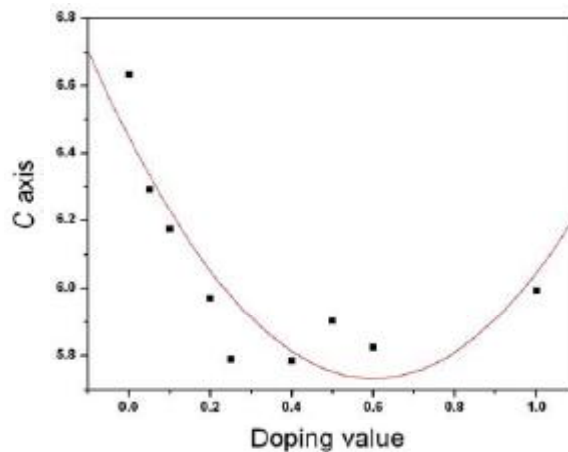


**Figure 2:** The relation between c-axis and doping value

hombic phase shifted and disappeared with  $x = 1$  indicating that the successful range of Cu-doped lies in between  $0.0 \leq x < 0.25$  which is fully consistent with most literature.

Figure (3<sub>a-d</sub>) Shows the SEM-micrographs recorded for pure and Cu-doped  $PbZrO_3$  with ( $x = 0.1, 0.5$  and 1 mole) which applied on the small species that prepared by solid state reaction route (SSR) and it shows the submicrometer and spherical nature of the

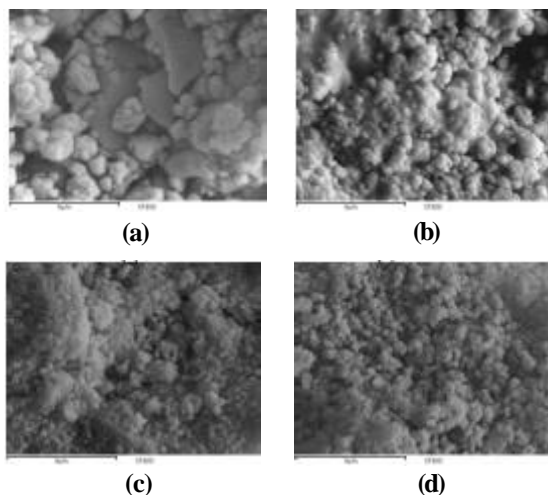


**Figure 3(a-d):** SE-micrographs for pure  $\text{PbZrO}_3$  and Cu-doped  $\text{Pb}_{1-x}\text{Cu}_x\text{ZrO}_3$  where (a)  $x=0$  mol, (b)  $x=0.1$  mol, (c)  $x=0.5$  mol and (d)  $x=1$  mol

$\text{PbZrO}_3$  powder. The average grain size was calculated and found in between 80 and 150 nm. These results are consistent with those results reported by Pai et al.<sup>[31]</sup> and Fang et al.<sup>[30]</sup> in which the conventionally  $\text{PbZrO}_3$  powder is covering the size range from 20 to 130 nm.

From figure (3<sub>a-d</sub>) it obviously that there is no large aggregations of the impurity phases were observed and at the same time there is no inhomogenieties in gray coloration degree that reflects the relative quality of preparation for measured samples.

Results of grains size analysis are partially agreement with data reported by<sup>[30-32]</sup> in point of view concerned by grain size, since our calculated average grain size is slightly smaller due to preparation conditions changments and Cu ions dopant element which make as splitter to the grain during the formation process specially at doping ratio  $0.25 \leq x < 1$ .

Figure (4<sub>a-k</sub>). Show the solid Infrared spectra for

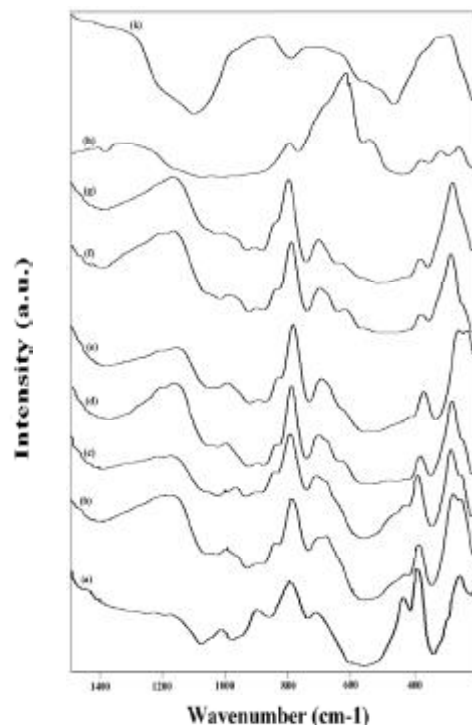


**Figure 4(a-k):** Solid Infrared Spectra for (a)  $\text{PbZrO}_3$ , (b)  $\text{Pb}_{0.95}\text{Cu}_{0.05}\text{ZrO}_3$ , (c)  $\text{Pb}_{0.9}\text{Cu}_{0.1}\text{ZrO}_3$ , (d)  $\text{Pb}_{0.8}\text{Cu}_{0.2}\text{ZrO}_3$ , (e)  $\text{Pb}_{0.75}\text{Cu}_{0.25}\text{ZrO}_3$ , (f)  $\text{Pb}_{0.6}\text{Cu}_{0.4}\text{ZrO}_3$ , (g)  $\text{Pb}_{0.5}\text{Cu}_{0.5}\text{ZrO}_3$ , (h)  $\text{Pb}_{0.4}\text{Cu}_{0.6}\text{ZrO}_3$ , (i)  $\text{CuZrO}_3$

pure and Cu-doped  $\text{PbZrO}_3$  powders, The spectra for pure  $\text{PbZrO}_3$  display bands at 225, 344 and 418  $\text{cm}^{-1}$  which have been assigned to  $\text{ZrO}_3$  torsions {see TABLE 1 } and those at 561 and 739  $\text{cm}^{-1}$  are due to Zr-O stretching and the other weak and very weak bands appearing at higher wavenumbers result from the valent oscillation of Metal-O bands<sup>[33]</sup>.

These results are in full agreement with those reported by<sup>[26]</sup> who were referring to the IR-spectra recorded for lead zirconate and specified types of vibrational modes that attributable to the different M-

**TABLE 1 : IR -absorption spectral bands recorded for the pure  $\text{PbZrO}_3$  and Cu-doped samples**

Materials	Wavenumber ( $\text{cm}^{-1}$ )											
$\text{PbZrO}_3$	225(m)	344(vs)	418(w)	561(b)	739(w)	866(w)	-	983(w)	1080(m)	1196(b)	-	1456(m)
$\text{Pb}_{0.95}\text{Cu}_{0.05}\text{ZrO}_3$	-	350(vs)	423(m)	559(b)	744(w)	836(m)	-	937(w)	1036(m)	-	1397(m)	-
$\text{Pb}_{0.9}\text{Cu}_{0.1}\text{ZrO}_3$	222(m)	348(vs)	423(w)	562(b)	745(s)	-	-	938(w)	1027(m)	-	1395(m)	-
$\text{Pb}_{0.8}\text{Cu}_{0.2}\text{ZrO}_3$	222(m)	355(s)	458(w)	531(w)	752(s)	838(m)	885(m)	936(m)	1034(m)	-	1380(m)	-
$\text{Pb}_{0.75}\text{Cu}_{0.25}\text{ZrO}_3$	223(w)	353(s)	-	564(m)	749(s)	-	886(m)	935(m)	1039(m)	-	1395(m)	-
$\text{Pb}_{0.6}\text{Cu}_{0.4}\text{ZrO}_3$	219(m)	361(w)	-	524(m)	750(s)	-	888(m)	935(m)	1028(m)	-	1399(m)	-
$\text{Pb}_{0.5}\text{Cu}_{0.5}\text{ZrO}_3$	221(m)	362(w)	-	522(m)	749(s)	-	888(m)	935(m)	1028(m)	-	1395(m)	-
$\text{Pb}_{0.4}\text{Cu}_{0.6}\text{ZrO}_3$	221(m)	328(w)	465(b)	585(m)	787(w)	-	-	-	1020(m)	-	1383(w)	-
$\text{CuZrO}_3$	221(m)	-	473(s)	-	799(w)	-	-	-	1050(b)	-	-	-
w =weak b =broad s =strong vs =very strong m=medium	-	-	-	-	-	-	-	-	-	-	-	

w =weak b =broad s =strong vs =very strong m=medium

## Full Paper

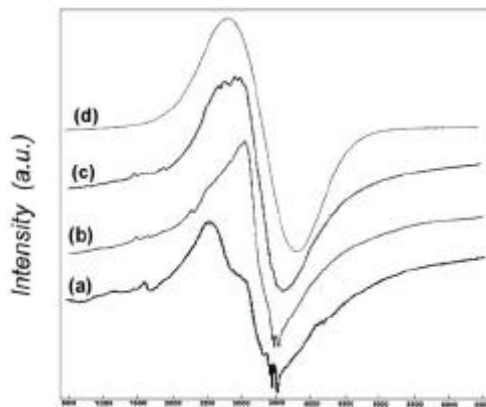


**Figure 5(a-d): ESR spectra at room temperature for pure  $PbZrO_3$  and Cu-doped  $Pb_{1-x}Cu_xZrO_3$  Where (a)  $x=0$  mol, (b)  $x=0.1$  mol, (c)  $x=0.5$  mol and (d)  $x=1$  mol**

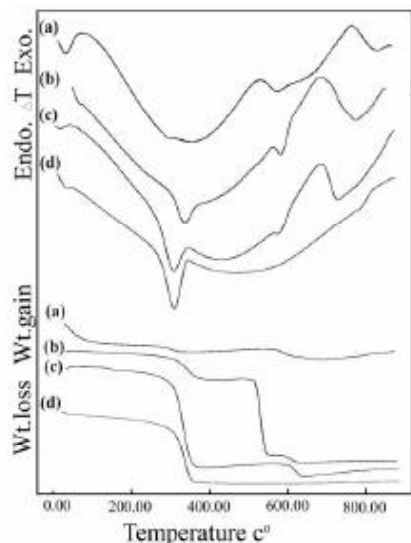


**Figure 6(a-d): Thermo gravimetric (TGA) and Differential thermal analyses (DTA) curves recorded for green mixture of pure  $PbZrO_3$  and Cu-doped  $Pb_{1-x}Cu_xZrO_3$  where (a)  $x=0$  mol, (b)  $x=0.1$  mol, (c)  $x=0.5$  mol and (d)  $x=1$  mol**

**TABLE 2 : The effective g-values ( $g_{iso}$ ) of some prepared samples of Cu-doped  $PbZrO_3$**

Material	$G_{iso}$ values
$PbZrO_3$	2.11
$Pb_{0.9}Cu_{0.1}ZrO_3$	2.282
$Pb_{0.5}Cu_{0.5}ZrO_3$	2.34
$CuZrO_3$	2.13

O vibrational modes inside rhombohedra structure and classified it into several ranges of spectra; I( $400-600\text{ cm}^{-1}$ ), II( $250-400\text{ cm}^{-1}$ ) and III( $150-250\text{ cm}^{-1}$ ). These strands of spectra appear in our recorded data for pure and Cu-doped lead zirconate.

Figure (5<sub>a-d</sub>). Display the electron-spin resonance

(ESR) signals recorded for pure and some selected Cu-doped  $PbZrO_3$  samples with ( $x=0.1, 0.5$  and  $1$  mole), the g-values parallel and perpendicular to the symmetry axis and the effective g-values which nominated as ( $g_{iso}$ ) are calculated as shown in TABLE 2. It is clearly that the effective g-values ( $g_{iso}$ ) exhibit an increase from  $x=0.0$  to  $x=0.5$  and decrease with  $x=1$  mole due to the strong coupling between  $Cu^{+2}$  ion that substitutes  $Pb^{+2}$  ion success fully at low dopant concentrations  $0.0 < x \leq 0.5$  while at higher concentration of doping range  $0.5 < x \leq 1$  copper in most cases as appear in our x-ray is out of crystalline lattice structure of lead zirconate.

These results of EPR is totally supported by<sup>[34,35]</sup> who investigated EPR-signals of doped  $BaTiO_3$  and some Cu-containing ceramic deducing that the anisotropy occurred as result of doped element and/or lattice defects could be the reason why g-effective varies as function of doping element.

The TGA and DTA analysis were carried out on the green mixtures of pure and Cu-doped  $PbZrO_3$  powders with ( $x=0.1, 0.5$  and  $1$  mole). From TGA/DTA curves figure (6<sub>a-d</sub>) The TGA analysis can be divided into steps.

The first step occupies the region from room temperature till  $230^{\circ}\text{C}$  for which the weight loss occurred is attributable to the humidity of samples and partial decomposition of  $CuCO_3$ . The second region lies from  $230-360^{\circ}\text{C}$  at which cupric carbonate decomposed completely into  $CuO$  plus  $CO_2$ .

The third region of temperature from  $360-410^{\circ}\text{C}$  at which the weight loss occurred attributable to the onset of the crystallization process.

These results are consistent with those reported by<sup>[36-38]</sup>. They mentioned that the broad/ slightly sharp exothermic peak that lies at ( $390-450^{\circ}\text{C}$ ) is revealed to the initial stage of phase formation of lead zirconate by additional to complete decomposition of  $CuCO_3$ .

From figure (6<sub>a-d</sub>) it is clear that the exothermic peak lies at  $\approx 400^{\circ}\text{C}$  begin to be sharp as Cu-dopant concentration increase from  $x=0.0$  till  $x=1$  mole which emphasize that this peak is mainly due to the  $CuCO_3$  decomposition<sup>[36]</sup>.

Figures (7<sub>a-d</sub>,8) show the conductivity-temperature curves plus conductivity as function of doping ratio respectively. It is clear that all samples exhibit semi conducting behaviors since conductivity decrease as tem-

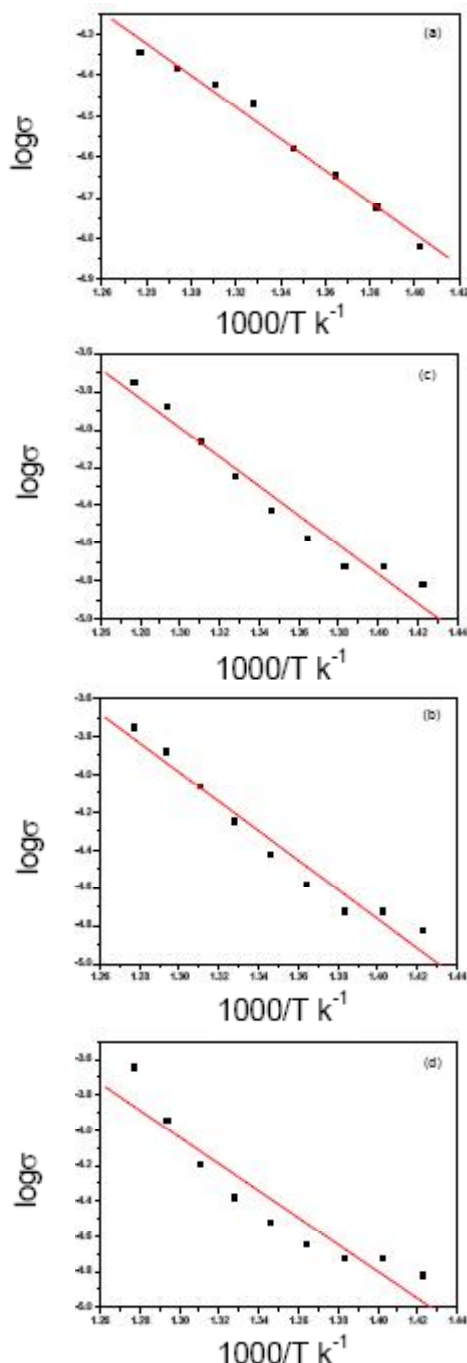


**Figure 7(a-d): The variation of DC-Electrical Conductivity as a function of temperature for (a)  $\text{PbZrO}_3$ , (b)  $\text{Pb}_{0.9}\text{Cu}_{0.1}\text{ZrO}_3$ , (c)  $\text{Pb}_{0.8}\text{Cu}_{0.2}\text{ZrO}_3$ , (d)  $\text{Pb}_{0.5}\text{Cu}_{0.5}\text{ZrO}_3$**

**TABLE 3 : The activation energy for pure  $\text{PbZrO}_3$  and some selected Cu-doped samples**

Material	Activation energy ( $\Delta E$ ) eV
$\text{PbZrO}_3$	$1.98 \times 10^{-4}$
$\text{Pb}_{0.9}\text{Cu}_{0.1}\text{ZrO}_3$	$4.47 \times 10^{-4}$
$\text{Pb}_{0.8}\text{Cu}_{0.2}\text{ZrO}_3$	$4.47 \times 10^{-4}$
$\text{Pb}_{0.5}\text{Cu}_{0.5}\text{ZrO}_3$	$4.31 \times 10^{-4}$

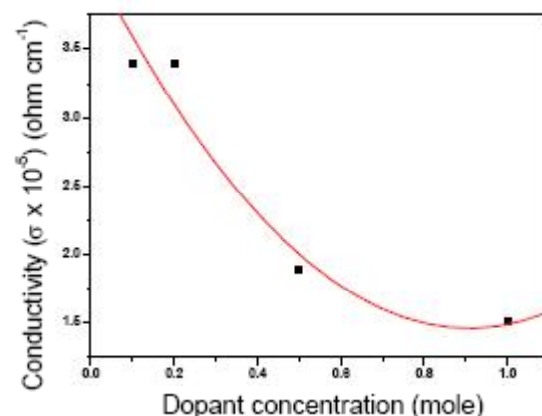


**Figure 8 : The variation of DC-Electrical conductivity as a function of Dopant concentration**

perature increase and the activation energy values were calculated {see TABLE (3)} which exhibiting an increase with  $x = 0.0$  mole till  $x = 0.2$  mole and slight decrease again at  $x \approx 0.25$  mole (optimum doping ratio).

It is well known that  $\text{PbZrO}_3$  crystal and ceramic usually contain vacancies in the Pb and O sub lattices due to  $\text{PbO}$  sublimation during preparation over temperature ( $650^\circ\text{C}$ ) that suffice for Pb-sublimation and as a result the electrical and conduction properties varies according to the amount of vacancies exist inside crystal structure of  $\text{PbZrO}_3$  [39-41].

Furthermore  $\text{PbZrO}_3$  regime is belonging to the p-type conductivity since  $\text{Pb}^{+2}$ /and  $\text{Cu}^{+2}$  iso-dopant element make as acceptor<sup>[42]</sup> that mean the conduction mechanism inside PZ-system occur through hole hopping mechanism, which enhancing by  $\text{Cu}^{+2}$  ion dopings as clear in figures (7<sub>a-d</sub>, 8).

For these results one can indicate that  $\text{Cu}^{+2}$  doping enhance conduction mechanism with out changing on the magnetic order of PZ or internal structure of this regime.

## CONCLUSIONS

The final conclusive remarks inside this article could be briefed in the following points:

1. Cu ions can be substitute successfully on the lead-site up to 0.25 mole.
2. The average grain size found to be in between 80 and 150 nm which confirmed that Cu-dopant make as splitter to the grain that reflects why this estimated

## Full Paper

- grain size is smaller than those mentioned on literature.
3. The most common vibrational modes those recorded for M-O (Zr-O) and (Pb-O) of perovskite which lies at 561 and 739cm<sup>-1</sup> respectively.
  4. Most of samples have the semi conducting behaviors and Cu ions dopings enhance the conduction mechanism of PZ-regime.
  5. The EPR signals recorded confirm that Cu-dopant increase the paramagnetic character of PbZrO<sub>3</sub> system and give a signal refers to Cu<sup>+</sup> ion existence.

## REFERENCES

- [1] R.Smoluchowski, N.Kurti; 'Solid State Physics: Structure, Properties and Preparation of Perovskite-Type Compounds', Pergamon Press Inc., **5**, 3-6,8,9,11 (1969).
- [2] A.Wold, K.Dwigh; 'Solid State Chemistry', Chapman and Hall Inc., **127**, 136,137 (1993).
- [3] J.F.Scott, C.A.Araujo; Science, **246**, 1400 (1989).
- [4] Y.H.Xu; Ferroelectric Materials and Their Applications, North-Holland, Amsterdam, 206 (1991).
- [5] R.Watton, P.Manning, Proc.SPIE, 3436, 541 (1998).
- [6] V.E.Wood, J.R.Bush, S.D.Ramamurthi, S.L.Swartz; J.Appl.Phys., **71**, 4557 (1992).
- [7] K.D.Preston, G.H.Haertling; Appl.Phys.Lett., **60**, 2831 (1992).
- [8] W.G.Liu, J.S.Ko, W.G.Zhu; Infrared Phys.Technol., **41**, 169 (2000).
- [9] D.Dimos, C.H.Muller; Annu.Rev.Mater.Sci., **28**, 397 (1998).
- [10] D.L.Polla; Microelectron.Eng., **29**, 51 (1995).
- [11] Y.Nemirovsky, A.Nemirovsky, P.Muralt, N.Setter; Sensors Actuators, **A56**, 239 (1996).
- [12] G.Heartling; J.Am.Ceram.Soc., **82**, 797 (1999).
- [13] K.Singh; Ferroelectrics, **94**, 433 (1989).
- [14] M.T.Lanagan, J.H.Kim, S.Jang, R.E.Newnham; J.Am.Ceram.Soc., **71**, 311 (1988).
- [15] K.Wakino, M.Murata,, H.Tamura; J.Am.Ceram. Soc., **69**, 34-37 (1986).
- [16] W.N.Lawless; Phys.Rev., **B30**, 6555-59 (1984).
- [17] D.M.Ibrahim, H.W.Hennie; Trans.J.Br.Ceram. Soc., **80**,18-22 (1981).
- [18] Y.S.Rao, C.S.Sunandana; J.Mater.Sci.Lett., **11**, 595-597 (1992).
- [19] E.E.Oren, E.Taspinar, A.C.Tas; J.Am.Ceram.Soc., **80(10)**, 2714-16 (1997).
- [20] J.Fang, J.Wang, S.C.Ng, L.M.Gan, C.H.Quek, C.H.Chew; Mater.Lett., **36**, 179-185 (1998).
- [21] B.Matthes, G.Tomandl, G.Werner; J.Eu.Ceram.Soc., **19(6-7)**, 1387-1389 (1999).
- [22] L.B.Kong, J.Ma, W.Zhu, O.K.Tan; Materials Letters, **49(2)**, 96-101 (2001).
- [23] S.S.N.Bharadwaja, S.B.Krupanidhi; Thin Solid Films, **423**, 88-96 (2003).
- [24] Z.G.Hu, F.W.Shi, T.Lin, Z.M.Huang, G.S.Wang, Y.N.Wu, J.H.Chu; Physics Letters, **A230**, 478-486 (2004).
- [25] Ahmed Boutarfaia, Ceramics International, **27**, 91-97 (2001).
- [26] A.I.Akimov, G.K.Savchuk,, T.M.Akimova; J.Appl. Spectrosc., **70(4)**, 498 (2003).
- [27] W.K.Han, J.W.Choi, G.H.Hwang, S.J.Hong, J.S. Lee, S.G.Kang; Applied Surface Science, **252(8)**, 2832 (2006).
- [28] H.D.Megaw; Proc.Phys.Soc.Lond., **58**, 133 (1946).
- [29] E.Sawaguchi, H.Maniwa, S.Hoshino; Phys.Rev., **53**, 1078 (1951).
- [30] J.Fang, J.Wang, S.C.Ng, L.M.Gan, C.H.Chew; Ceramic International 24 (1998).
- [31] Rajesh V.Pai, T.V.Vittal Rao, Ashok Kumar, S.K. Mukerjee, V.Venugopal; Journal of Alloys and Compounds, 443 (2007).
- [32] S.Sharma, R.Singh, T.C.Goel, S.Chandra; Computational Materials Science, **37**, 86 (2006).
- [33] C.Rao; Academic Press, 356 (1963).
- [34] I.Onyszkiewicz, P.Czarnecki, R.Micnas, S. Robaszkiewicz; Physica (B+C) **147(2-3)**, 166 (1988).
- [35] T.Hidaka; Phys.Rev., **B20**, 2769 (1979).
- [36] M.M.A.Sekkina, K.M.Elsabawy; Physica, **C377**, 254 (2002).
- [37] Y.Srinivasa Rao, C.S.Sunandana; J.Materials Science Letters, 11, (1992).
- [38] R.H.Tahar, N.H.Tahar, A.B.Salah; J.Crystal Growth, 307 (2007).
- [39] Z.Ujma, J.Hañderek; J.Phase Transitions, **3**, 121 (1983).
- [40] Z.Ujma; J.Phase Transitions, **4**, 169 (1984).
- [41] Z.Ujma, D.Dmytrów, J.Hañderek; Ferroelectrics, **81**, 107 (1988).
- [42] Z.Ujma, J.Hañderek; Phys.Stat.Sol., **A28**, 489 (1975).